# ISTITUTO NAZIONALE DI FISICA NUCLEARE

**Sezione di Milano**

---

**INFN/AE-92/06**
**21 Febbraio 1992**



S. Bonetti, I. Manno, A. Preda, P. Ullucci:


## EVENT SIMULATION AND RECONSTRUCTION IN BOREXINO


**Servizio Documentazione**
dei Laboratori Nazionali di Frascati

INFN - ISTITUTO NAZIONALE DI FISICA NUCLEARE
Sezione di Milano

INFN/AE-92/06
21 Febbraio 1992

# EVENT SIMULATION AND RECONSTRUCTION IN BOREXINO

*S.Bonetti, I.Manno, A.Preda, P.Ullucci*
*Physics Department of University and INFN - Milano*

## ABSTRACT

Solar neutrinos on the Earth induce interactions where electrons and gammas are produced. Due to the involved energy region, beta and gamma radioactive decays of any material are source of background: therefore very important is the knowledge of both neutrino signal and background event configuration. The simulation of electromagnetic shower production, their propagation inside a liquid scintillator and their reconstruction in a spectroscopic real time detector like Borexino are presented in this paper.

## 1 - INTRODUCTION

BOREXINO is an experiment conceived with the aim to investigate the flux and the properties of neutrinos born inside the Sun [Ref. 1].

The basic design of the Borexino detector is simply described: a central spherical volume of liquid scintillator will be observed by a large number of concentrically distributed phototubes. An overall shielding architecture protects the scintillator volume from background radiations from the rock as well as contamination in the shielding and container materials.

The cardinal aspects of the design are: detection of the scintillation signal (determining the fiducial target volume (*F.V.*) and the optical coverage of the emitted scintillation light, thus also the number of phototubes (*PMT*)/reflector units and the radius of the *PMT* surface), the shielding architecture (determining the dimensions of the containment vessels for the scintillator and other shielding liquids) and finally, interwoven in the above, radioactive purity aspects of all materials other than the liquid scintillator.

The overall size of Borexino is decided by two basic dimensions: a) the target volume will be 100 tons scintillator mixture: trimethylborate (*TMB* i.e. $B(OCH_3)_3$) + pseudocumene (*PC* i.e. $C_6H_3(CH_3)_3$) with the *TMB* at a concentration level ranging from 80% to 90% by weight; thus with a density of $\sim 0.9 g/cm^3$, this results in a *F.V.* sphere of 6 m diameter; b) it is necessary to arrange a total shielding depth of ~5 mwe to protect the *F.V.* from the rock backgrounds. Details of the detector are arranged by these two limiting dimensions.

The individual components of the detector are: 1) the inner container vessel (*I.V.*) holding the liquid scintillator. Its total mass is ~300 tons, thus the radius of this vessel is 4.25 m, the outer 1.25 m serving as the last shielding buffer for the *F.V.* also with respect to the shielding water and the inner container material. The container is made of teflon laminated acrylic, the transparency of which permits observation of the scintillations. 2) The *PMT* array placed at the diameter of 12.5 m. The scintillation vessel is completely submerged in a containment tank of diameter 17 m filled with water. The water provides the final ~4 m shielding from the rock ambience. In this design, the *PMT*/reflector array is thus immersed in water.

## 2 - NEUTRINO SIGNAL AND BACKGROUND

The main sources of neutrino production inside the Sun are the "p-p" reaction, the $^7$Be capture and the $^8$B decay, involving different energy regions: the maximum energy of $\nu$ produced in the p-p source is 0.42 MeV, in the $^8$B decay is 15 MeV, and $^7$Be is a double monochromatic source of energy $E_1$=0.383 MeV, $E_2$=0.861 MeV. The sensitivity of Borexino is expected to be very high for the $^7$Be neutrinos, and sufficient also for the $^8$B ones; the possibility of observing neutrinos originated from the p-p source is ruled out by the background high rate in this so low energy region.

The interactions induced by solar neutrinos are mainly due to elastic scattering on electron target

$$\nu + e^- \rightarrow \nu + e^-$$

where an electron of energy ranging from 0 to 15 MeV is produced in the final state; moreover the inverse-beta decay of the $^{11}$B is expected

$$\nu + {}^{11}\mathrm{B} \rightarrow e^- + [{}^{11}\mathrm{C}^* \rightarrow \gamma + {}^{11}\mathrm{C}]$$

where an electron and a possible gamma, with a total event energy in the range 0 - 13 MeV, are present in the final state. Therefore any interaction involving an electron or a gamma in this energy range could be a "neutrino-candidate" : events induced by the natural radioactivity in the scintillator or in the material surrounding it are in effect sources of background in the neutrino signal detection.

The production and the propagation of the showers originated by electrons and gammas inside the scintillator, the light generation in it, its collection on the photomultipliers, and finally the reconstruction of the event energy and position have been studied in the assumed configuration of Borexino.

It has to be stressed that, from the point of view of the e.m. shower generation and propagation, the difference between a pure $TMB$ scintillator or a mixture like $TMB + PC$ is negligible.

The signal and background events have been simulated by means of a Monte Carlo program: here a summarized description of this code is reported; in particular the assumed hypotheses and methods used in the reconstruction of the events are presented with some detail. Results of the simulations are reported mainly for electrons and gammas of typical energies in our region of interest.

It can be noted that the problematic of the Borexino simulations is common to any experiment operating in the research of rare events in the energy region of the solar neutrinos by a scintillator or Čerenkov technique, where the energy and space resolution are very important in order to reject the background.

## 3 - THE MONTE CARLO STRUCTURE

The generation, simulation and reconstruction of the events in Borexino has been performed by the Monte Carlo code *CRONOS* (Code for Reconstruction Of Neutrino Observed Signal). It is composed of two programs: *GENEB* (GEneration of NEutrino and Background interactions) and *SRSE* (Simulation and Reconstruction of Scintillation Events). *GENEB* provides a detailed and complete study of the electromagnetic showers produced by the electrons and gammas inside Borexino with the aid of the *EGS* code [Ref. 2]. *SRSE* consists of two main parts: the first part is a Monte Carlo program which simulates the detector signals from the energy deposit of all the tracks in the scintillator; the second part reconstructs the events from the signals.

## 4 - TOPOLOGY OF THE EVENTS

As recalled in §2 the interactions produced by solar neutrinos consist of electrons and gammas with an energy ranging from 0 to 15 MeV. The natural radioactivity of the scintillator and of all materials composing and surrounding the detector produces events with electrons, gammas and alphas in the final state; their energy ranges are: 0 - 5 MeV for betas and gammas and 3 - 8 MeV for alphas.

A study of the electromagnetic showers produced by these electrons and photons has been made by means of the *EGS* code; its structure allows to perform a detailed description of the space-time development of the shower and of the energy deposits.

Due to the finite resolution of the spatial reconstruction, a track shorter than 5 cm is considered as a point like deposit of energy. Due to the range-energy relation in *TMB* liquid, 5 cm is the maximum track length for any electron produced either directly from the primary interaction or through a shower development. The space-time development of the showers is strictly followed, according to a sort of "quantisation" criterion: a shower induced by a photon is described as a set of points, each of them characterized by an energy deposit and by the space-time coordinates of each charged particle, while the energy released by a primary electron, which does not produce Bremsstrahlung, is associated to a single point.

Every secondary particle is tagged according to the physics process: Compton electron, Bremsstrahlung photon, etc. The only tracks which do not follow this procedure are the Moller and Bhabha electrons due to their low energy and short range; their energy deposits are included in the calculation of the total energy lost by their "father" electron or positron. In the processing of the showers a lower energy threshold of 10 keV and 5 keV are assumed for electrons and photons, respectively.

The most important physics parameters involved in the electron and photon propagation are shown in Figs. 1-3 and in Tabs. I and II. We can stress the following observations:

- the value of the total cross section for the electrons is stable in the energy region 1 - 20 MeV at ~1.300 barn/molecule (Fig. 1);
- the ionization energy loss is steeply decreasing between 10 keV and 1 MeV, while it is steady at ~1.3 MeV/cm in the energy range 1 - 20 MeV. The energy loss due to the ionization is dominant with respect to the radiation loss (Fig. 2);
- the cross section for Bremsstrahlung is only 2.5% of the total cross section at 5 MeV (Tab. I);
- the mean free path for a photon conversion corresponding to a 5 MeV energy is ~37 cm (Fig. 3); the radiation length is ~43. cm;
- in the energy range of this experiment the photon interacts predominantly through the Compton scattering, which represents ~ 100% of the total cross section between 400 and 900 keV and ~ 85% from 5 to 10 MeV (Table II).

The distribution of the number of Compton electrons is shown in Fig. 4; their number per shower is, on the average, ~20 at 5 MeV. In Figs. 5a and 5b the distribution of the number of Moller electrons and Bremsstrahlung photons per incident electron are represented. One radiation photon is produced only in ~ 30% of the showers, while two photons are produced only the ~ 7% of times (for $E_e$= 5 MeV).

The maximum longitudinal extension of the shower for photons and electrons is displayed in Figs. 6a and 6b: the 80% of all electron showers are shorter than 5 cm while the 70% of the photons showers are in the range 10 - 50 cm and the 10% is longer than 1 m. In addition the energy losses are concentrated in the origin of the electron showers while the ~ 90% are lost in 50 cm for the photon showers (see Figs.

7a, 7b and 8a, 8b). The energy deposits by a single 5 MeV photon in a parallel plane with respect to the incident direction is shown in Fig. 9.

Antineutrino interactions with the consequent possible production of positrons have been simulated. Due to the initial annihilation process the energy deposit through the shower is symmetric with respect to the origin. In addition the maximum extension of the shower is larger than in the case of electrons ($\sim$ 35 cm is the most probable value) (see Figs. 10a and 10b).

*Table I: Branching ratio (B.R.) of the Bremsstrahlung cross section relative to the total cross section for electrons in the energy range 0.6 - 20. MeV in TMB.*

| TOT EN. (MeV) | B.R. |
|---|---|
| 0.604 | 5.4E-03 |
| 0.619 | 6.0E-03 |
| 0.637 | 6.6E-03 |
| 0.658 | 7.3E-03 |
| 0.682 | 8.0E-03 |
| 0.710 | 8.8E-03 |
| 0.743 | 9.6E-03 |
| 0.782 | 1.0E-02 |
| 0.827 | 1.1E-02 |
| 0.879 | 1.2E-02 |
| 0.939 | 1.3E-02 |
| 1.010 | 1.4E-02 |
| 1.092 | 1.5E-02 |
| 1.188 | 1.6E-02 |
| 1.300 | 1.7E-02 |
| 1.431 | 1.8E-02 |
| 1.582 | 1.9E-02 |
| 1.759 | 1.9E-02 |
| 1.965 | 2.0E-02 |
| 2.205 | 2.1E-02 |
| 2.484 | 2.1E-02 |
| 2.810 | 2.2E-02 |
| 3.189 | 2.2E-02 |
| 3.631 | 2.3E-02 |
| 4.145 | 2.3E-02 |
| 4.745 | 2.4E-02 |
| 5.443 | 2.5E-02 |
| 6.257 | 2.5E-02 |
| 7.205 | 2.6E-02 |
| 8.309 | 2.7E-02 |
| 9.595 | 2.7E-02 |
| 11.093 | 2.8E-02 |
| 12.838 | 2.9E-02 |
| 14.872 | 3.0E-02 |
| 17.240 | 3.0E-02 |
| 20.000 | 3.1E-02 |

*Table II: Branching ratio (B.R.) of the Compton cross section relative to the total cross section for photons in the energy range 0.005 - 20. MeV in TMB.*

| EN (MeV) | B.R. |
|---|---|
| 4.99E-03 | 7.1E-03 |
| 5.92E-03 | 1.1E-02 |
| 7.01E-03 | 2.0E-02 |
| 8.30E-03 | 3.4E-02 |
| 9.84E-03 | 5.7E-02 |
| 1.16E-02 | 9.3E-02 |
| 1.38E-02 | 0.14 |
| 1.63E-02 | 0.23 |
| 1.93E-02 | 0.33 |
| 2.29E-02 | 0.46 |
| 2.71E-02 | 0.59 |
| 3.21E-02 | 0.71 |
| 3.81E-02 | 0.81 |
| 4.51E-02 | 0.88 |
| 5.34E-02 | 0.92 |
| 6.33E-02 | 0.95 |
| 7.50E-02 | 0.97 |
| 8.88E-02 | 0.98 |
| 0.105 | 0.99 |
| 0.124 | 0.99 |
| 0.147 | 0.99 |
| 0.174 | 0.99 |
| 0.207 | 0.99 |
| 0.245 | 0.99 |
| 0.290 | 0.99 |
| 0.344 | 0.99 |
| 0.407 | 1.00 |
| 0.482 | 1.00 |
| 0.571 | 1.00 |
| 0.677 | 1.00 |
| 0.802 | 1.00 |
| 0.950 | 1.00 |
| 1.125 | 0.99 |
| 1.333 | 0.99 |
| 1.578 | 0.99 |
| 1.870 | 0.99 |
| 2.215 | 0.98 |
| 2.623 | 0.98 |
| 3.107 | 0.97 |
| 3.680 | 0.95 |
| 4.359 | 0.93 |
| 5.163 | 0.91 |
| 6.115 | 0.89 |
| 7.243 | 0.85 |
| 8.579 | 0.82 |
| 10.162 | 0.78 |
| 12.036 | 0.73 |
| 14.256 | 0.68 |
| 16.885 | 0.63 |
| 20.000 | 0.58 |

## 5 - BASIC PHENOMENA IN SCINTILLATION DETECTORS

The Simulation and Reconstruction of Scintillation Event ($SRSE$) program has two main parts. The first part is a Monte Carlo program which simulates the $PMT$ signals from the energy deposits of the scintillation event. The second part of the program reconstructs the space-time coordinates and the energy of the event from the $PMT$ signals produced by the energy deposits. In this paragraph there is a short description of the physical phenomena which have to be taken into account during the simulation procedure.

### 5.1 - PHOTON YIELD

The photomultiplier tubes detect photons produced by two phenomena in the detector volume: the scintillation light produced by charged particles in the scintillator and the Čerenkov radiation of fast charged particles.

The scintillation photon yield is about 4850 photons/MeV in the scintillator, which will be used in Borexino. The scintillation photons are emitted isotropically where the energy is deposited.

The analysis of the measured spectra has shown that the best approximation of the decay spectra is given by the sum of three exponentials:

$$f(t) = e^{(p_1+p_2 t)} + e^{(p_3+p_4 t)} + e^{(p_5+p_6 t)} .$$

The decay time and the relative contribution of the components are given by:

$$\int_0^\infty f(t)dt = -\frac{e^{p_1}}{p_2} - \frac{e^{p_3}}{p_4} - \frac{e^{p_5}}{p_6} = A ,$$

$$\tau_i = -\frac{1}{p_{2i}} \qquad \text{and} \qquad q_i = -\frac{e^{p_i}}{A p_{2i}} .$$

where $\tau_i$ and $q_i$ are the decay time and the relative contribution of the $i$-th component and A is the area below the decay curve. In Figs. 11 the sum of three exponentials is fitted to the decay curve of excitations produced by gamma rays (it is the same for electrons), while in Fig. 12 the sum of three exponentials is fitted to the decay curve of excitations produced by $\alpha$ particles and in Fig. 13 the two fitted curves are shown.

A scintillation event consists of one or more energy deposits. Each energy deposit is characterized by the time $t_i$ when the energy is deposited, by the space vector $\vec{r}_i$ and by the $E_i$ deposited energy. The number of generated scintillation photons is proportional to the deposited energy. They are emitted isotropically.

The centre of gravity of the energy deposits is given by:

$$\vec{r}_c = \frac{\sum \vec{r}_i E_i}{\sum E_i} ,$$

where $\vec{r}_i$ is the space vector of the $i$-th energy deposit and $E_i$ is the deposited energy. The spatial spread of the energy deposits is given by:

$$\sigma_r = \sqrt{\frac{\sum(\vec{r}_i - \vec{r}_c)^2 E_i}{\sum E_i}}$$

The time spread of the energy deposits is given by:

$$\sigma_t = \sqrt{\frac{\sum(t_i - \bar{t})^2 E_i}{\sum E_i}} ,$$

where $E_i$ is the quantity of the $i$-th energy deposited at time $t_i$. $\bar{t}$ is the mean of the energy deposit times:

$$\bar{t} = \frac{\sum t_i E_i}{\sum E_i} .$$

The distributions of the energy deposits produced by electrons and gamma rays are different. In Figs. 14 and 15 the distributions of these values are shown for events produced by 5 MeV electrons and for 5 MeV gamma rays, respectively.

As it is well known, the Čerenkov radiation is emitted at an angle $\theta$ with respect to the direction of motion of the charged particle, thus forming a conical wave front:

$$\cos\theta = \frac{1}{\beta n} ,$$

where $\beta = v/c$, $n$ is the refractive index of the media, $v$ is the speed of the charged particle and $c$ is the speed of light. The number of emitted photons per cm of path length is given by:

$$N = \frac{\alpha}{c} \int \left(1 - \frac{1}{\beta^2 n^2}\right) 2\pi d\nu ,$$

where $\alpha$ is the fine structure constant ($a = 1/137$). In the case of visible spectrum:

$$N \sim 500 \sin^2\theta/cm .$$

In the Borexino detector, the Čerenkov radiation is emitted by muons passing through the buffer space filled with water between the photomultiplier tubes and the inner vessel. Detecting this Čerenkov radiation could be useful in recognising background events produced by muons in the water.

## 5.2 - PROPAGATION OF ELECTROMAGNETIC RADIATION

The propagation of the electromagnetic radiation in transparent media is described by optical laws. When an electromagnetic radiation passes from one transparent medium to another it is reflected and refracted. The amount of reflected and transmitted electromagnetic radiation is described by the reflectivity $r$ and transmissivity $t$, respectively. One may calculate the reflectivity and transmissivity from the Fresnel formulae [Ref. 3]:

$$r = \frac{|R|^2}{|A|^2}$$

and

$$t = \frac{n_2 \cos\theta_t |T|^2}{n_1 \cos\theta_i |A|^2} .$$

where $n_1$ and $n_2$ are the refractive indices of the two media, $A$ is the amplitude of the electric vector of the incident wave, $R$ and $T$ are the amplitides of the reflected and the transmitted waves, $\theta_i$ is the angle of incidence and $\theta_t$ is the angle of refraction.

When the electromagnetic radiation strikes a surface of separation of two different media, some is thrown back into the original medium. The direction of the reflected and refracted light is given by:

$$\vec{v}_r = \vec{v}_i - 2(\vec{v}_i\vec{n})\vec{n} \ ,$$

and

$$\vec{v}_t = \vec{v}_i \cos\theta_t + (\vec{v}_i - \vec{n}\cos\theta_i)\frac{n_1}{n_2} \ .$$

where $v_i$, $v_r$ and $v_t$ are the directions of the incident, reflected and transmitted light, respectively, and $\vec{n}$ is the vector perpendicular to the surface in the point of incidence. If $\sin\theta_i \geq n_2/n_1$, the light is totally reflected.

During its passage through a medium the electromagnetic radiation is absorbed to an extent that depends on the wavelength of the radiation, the thickness and the nature of the medium. If $d\Phi$ is the change in the monochromatic radiation flux in passing through a small thickness dl of an absorbing medium, then:

$$a = \frac{1}{\Phi}\frac{d\Phi}{dl}, \qquad \text{i.e.} \qquad \frac{\Phi_x}{\Phi_0} = e^{-ax},$$

where $\Phi_0$ is the initial flux, $\Phi_x$ the flux after a distance $x$ and $a$ is the absorption coefficient.

The photons are scattered in the transparent media (liquid scintillator, pseudocumene, water etc.). This light scattering is characterized by the light scattering mean free path length and by the probability density function of the scattering angle.

The spread of the photon transit times due to the light scattering has a significant influence on the reconstruction accuracy.

## 6 - DETECTOR PARAMETERS

The $SRSE$ program can work with detectors of different sizes and shapes. The $SRSE$ parameters for the Borexino detector are summarised in Table III.

The typical detector consists of a vessel filled with liquid scintillator which is watched by photomultiplier tubes ($PMT$). In the program the scintillator is characterized by the scintillation photon yield, by the attenuation of the scintillation light, by the light scattering etc. A photomultiplier tube is characterized by its position and direction, by the size and shape and the quantum efficiency of its photocathode, by its time jitter, by the practical coefficient etc. Light guides ($LG$) collect the scintillation light. A light guide is characterized by its shape and by the reflection coefficient of its surface.

In a spherical detector, the $LG + PMT$ systems are placed on the surface of a sphere. In the simplest case, the $LG + PMT$ systems are placed along circles on the sphere. It is possible to construct arrangements which have the same symmetrical properties as the symmetrical solid bodies (tetraeder, cube, octaeder, dodecaeder and ikozaeder). The $z$-axis of the detector coordinate system is vertical and the origin of the coordinate system coincides with the detector centre.

Table III. Parameters of the Borexino detector used in the $SRSE$ program.

| *Liquid Scintillator (sample D2)* | |
|---|---|
| Refractive index ($n$) | 1.4 |
| Attenuation length | 14.5 m |
| Scintillation photon yield | 4853photons/MeV |
| Light scattering mean free path length | 25 m |
| *THORN EMI 9351KB Photo Tubes* | |
| Number of $PMT$'s | 1658 |
| $PMT$ photocathode radius ($R_1$) | 0.095 m |
| $PMT$ photocathode curvature ($R_2$) | 0.110 m |
| $PMT$ time jitter ($\sigma$) | 1 ns |
| $PMT$ quantum efficiency ($q$) | 20 % |
| Practical coefficient | 0.6 |
| *Parabola-Shaped Light Guide* | |
| $LG$ minimum radius ($R_n = R_1$) | 0.095 m |
| $LG$ maximum radius ($R_x = 2.1R_n$) | 0.1995m |
| $LG$ length | 0.5m |
| $LG$ reflection coefficient | 0.9 |
| *Detector Dimensions* | |
| Fiducial Volume ($F.V.$) diameter | 6 m |
| Inner Vessel ($I.V.$) diameter | 8.5 m |
| Thickness of the acrylic wall | 0.02 m |
| Distance of $PMT$'s from center | 6.25 m |
| Distance of $LG$ entrance from center | 5.75 m |

## 6.1 - PHOTOMULTIPLIER TUBES

The shape of the photomultiplier tube's photocathode is a spherical section. This surface is described by the $R_1$ radius of the photocathode (the spherical section) and by the $R_2$ curvature of the surface. The $z$-axis of the coordinate system of the photocathode crosses the photocathode at its centre and the centre of the sphere of the photocathode coincides with the origin of the coordinate system.

## 6.2 - LIGHT GUIDES

The scintillation light emerging from the spherical inner vessel is guided to the photomultiplier tubes by light guides ($LG$) which improve the amount of light collected by the photomultiplier tubes. The $xy$-plane of the $LG$ coordinate system coincides with the plane where the photons enter into the $LG$ and it is perpendicular to the $LG$ axis. The origin of the coordinate system is on the $LG$ axis; the $z$-axis coincides with the $LG$ axis and it points from the photocathode to the $LG$ entrance. The $LG$ is a surface of a revolution body. Its length is L and its minimum radius is equal to the photocathode radius ($R_n = R_1$). Different shapes (Cone, Barrel, Parabola and Half-Barrel) have been studied.

Parabola-Shaped *LG*. The *LG* is a surface of revolution of a parabola about its axis (Fig. 16). The maximum radius of the *LG* is at the end where the scintillation photons enter the *LG* ($R_x$). The equation of the *LG* surface is given by:

$$z = a(x^2 + y^2) + b \ ,$$

where:

$$a = \frac{L}{R_x^2 - R_n^2} \qquad \text{and} \qquad b = \frac{-LR_x}{R_x^2 - R_n^2} \ .$$

The light collections of light guides of different shapes are shown in Table IV. There are no significant differences between the different shapes.

Table IV. Light collection of the different light guides.

| The length of the each light guides is 0.5m | | | | |
|---|---|---|---|---|
| $R_x$ (cm) | Coverage (%) | Half-Barrel *LG* (p.e.) | Parabola *LG* (p.e.) | Cone *LG* (p.e.) |
| 14.25 | 25.46 | 63 | 69 | 70 |
| 19.95 | 49.90 | 153 | 171 | 173 |
| 23.75 | 70.72 | 213 | 244 | 230 |

| The length of the each light guides is 1.0m | | | | |
|---|---|---|---|---|
| $R_x$ (cm) | Coverage (%) | Half-Barrel *LG* (p.e.) | Parabola *LG* (p.e.) | Cone *LG* (p.e.) |
| 14.25 | 30.54 | 106 | 107 | 107 |
| 19.95 | 59.85 | 190 | 200 | 206 |
| 23.75 | 84.83 | 266 | 293 | 283 |

The 1 MeV point-sized energy deposits were uniformly distributed in the *F.V.* of Borexino and the produced photo electrons (p.e.) were counted. In each case 1000 energy deposits were simulated.

## 6.3 - TRIGGER

A good event is a coincidence of $n$ *PMT* signals within a $\Delta T$ interval. The total number of *PMT*'s is $N$. The *PMT* thresholds are set usually at 0.3 photo electron level. The dark counting rate in each *PMT* is $r$ at this level. The $n$ is defined in such a way that the random $n$-fold coincidence rate from dark counts is negligible. $\Delta T$ should be, at least, as long as the maximum of the scintillation photon flight times. In the case of a spherical detector:

$$\Delta T = \frac{2Rn}{c} + \Delta T_{LG} \ ,$$

where $R$ is the radius of the spherical detector, $n$ is the refractive index of the liquid scintillator, c is the speed of light and $\Delta T_{LG}$ is the difference between the

maximum and the minimum of the photon flight times through the light guides. If each scintillation photon flies along a straight line from the point where it is produced to the $PMT$ where it is detected, then the t time of flight of the scintillation photon has the limits:

$$\frac{(R-r)n}{c} < t < \frac{(R+r)n}{c} ,$$

where $r$ is the distance between the detector centre and the energy deposit and $n$ is the refractive index of the liquid scintillator. The time of flight of the photons through the light guide varies from a minimum value (when the photon is flying along the light guide axis) to a maximum value (when the trajectory of the photon ecloses a large angle with the light guide axis).

## 6.4 - COORDINATE SYSTEMS

The program uses several coordinate systems. The detector has its own coordinate system and each $LG + PMT$ unit has a coordinate system too.

Detector Coordinate Systems: the $z$-axis of the coordinate system coincides with the symmetry axis of the detector and its origin is in the centre of the detector. If the shape of the detector is a sphere the $z$-axis is vertical.

$LG+PMT$ Coordinate Systems: each $LG+PMT$ system has its own coordinate system. The $z$-axis of the coordinate system coincides with the axis of the $LG+PMT$ system. The $z$-axis points from the photocathode to the entrance of the $LG$. The $xy$-plane of the $LG + PMT$ coordinate system coincides with the plane of the $LG$ entrance.

The communication is performed by coordinate transformations between different coordinate systems (Fig. 17).

## 7 - EVENT SIMULATION

In Borexino an event consists of one or more energy deposits. One may consider that the energy deposits are point-sized (if an energy deposit has an extension, one may divide it into smaller parts in such a way that the extension of each part should be negligible). Each energy deposit is characterized by the time when the energy is deposited, by the space coordinates of the energy deposit and by the quantity of the deposited energy. The energy deposits are processed one by one. The number of scintillation photons produced by each energy deposit is determined; they are emitted isotropically. The fast charged particles emit Čerenkov radiation too. Each photon is tracked from the place where it is produced to the place where it is absorbed or detected. In the tracking procedure the scintillation decay, the light scattering, the light collection efficiency of the light guides, the quantum efficiency and the time jitter of the $PMT$'s as well as the reflection and refraction at boundary layersare taken into account. If the scintillation photon is detected its contribution to the detector signals is determined. A detected scintillation photon is characterized by the time and by the place ($PMT$ position) of its detection.

## 7.1 - *PMT* SIGNALS

The photons produced by an event in the sensitive volume of Borexino generate *PMT* signals. The number of detected photons and the number of hit *PMT*'s depend on the deposited energy and on the space coordinates of the energy deposit (Table V).

Table V. The number of detected photons and the number of hit *PMT*'s.

| Photo electrons and *PMT*'s per event | | |
|---|---|---|
| Energy (MeV) | p.e./event$\pm\sigma$ | *PMT*'s/event$\pm\sigma$ |
| 0.05 | 9.3±3.0 | 9.3±3.0 |
| 0.1 | 18.8±4.2 | 18.6±4.2 |
| 0.2 | 36.8±5.8 | 36.1±5.6 |
| 0.5 | 93.6±9.2 | 89.4±8.5 |
| 1.0 | 188.2±14.0 | 171.8±12.1 |
| 2.0 | 375.8±20.3 | 315.5±16.3 |
| 4.0 | 750.3±30.3 | 545.5±28.0 |
| 5.0 | 939.0±35.5 | 639.3±33.4 |
| 6.0 | 1125.0±38.8 | 723.7±41.4 |

The events were uniformly distributed in the fiducial volume of Borexino.

These *PMT* signals provide information on the times when the *PMT*'s detect the photons (time signals) and on the number of *PMT*'s which give a signal. The time when the *PMT* detects a photon depends: 1) on the time when the photon was produced, 2) on the time of flight of the photon from its birth-place to the *PMT* and 3) on the *PMT* time jitter. In case of scintillation photons the birth of the photon is delayed by the scintillation decay.

## 8 - EVENT DISPLAY

The time signals of the event are plotted vs. their positions. In the case of spherical detector the positions of the photomultiplier tubes are given in polar coordinates $(\varphi, \vartheta)$. A three-dimensional event is projected in a plane with the

$$u = -x\sin\varphi + y\cos\varphi$$

and

$$v = -\cos\vartheta(x\cos\varphi + y\sin\varphi) + z\sin\vartheta$$

formulae to get a quasi three-dimensional display. In Fig. 18 a 500 keV point-sized energy deposit is displayed. It is worth to note that, as an example, one can recognize easily on the event display the distribution of the *PMT* pulses which correspond to the Čerenkov radiation of a muon passing through the water of the buffer space. It emits the photons along a cone with respect to the its fly direction.

## 9 - EVENT RECONSTRUCTION

The space-time coordinates of an event and the deposited energy are reconstructed from the *PMT* signals produced by the event.

1) The space-time coordinates of an event are calculated with the maximum likelihood method from the *PMT* time signals (vertex reconstruction). In Fig. 19 the $\Delta r$ vertex error is displayed for 100 keV, 500 keV, 2 MeV and 5 MeV point-sized energy deposits, respectively. The events are distributed uniformly in the fiducial volume of Borexino. In Fig. 20 the error of the coordinates and energy reconstruction for 500 keV electrons are shown.

2) The energy deposit is determined by means of a look-up table (Fig. 21). The number of *PMT* signals depends on the space coordinates of the energy deposits and on the deposited energy:

$$N_{PMT} = f(\vec{r}_e, E) \ ,$$

where $E$ is the deposited energy, $\vec{r}_e$ is the space vector of the energy deposit and $N_{PMT}$ is the number of *PMT* signals. This table is calculated with Monte Carlo method in the program. Then it is possible to give:

$$E = T(N_{PMT}, \vec{r}_e)$$

(Fig. 21) and determine the deposited energy from the number of *PMT* signals and the reconstructed space coordinates of the energy deposit. The results of the energy reconstructions are shown in Fig. 22. The simulated events have deposited 100 keV, 500 keV, 1 MeV and 2 MeV energy in the liquid scintillator and they were distributed uniformly in the fiducial volume.

### 9.1 - SPATIAL AND ENERGY RESOLUTION

The parameters of the event (time, position, energy etc.) are reconstructed from the *PMT* signals. The accuracy of the vertex reconstruction is limited by the error of the time signals. In Borexino the spatial error of one time signal is about 1 m. So according to statistical laws at least 100 time signals are needed to reduce to 10 cm the error of the localization based on time signals. The Borexino resolutions are shown in Table VI.

Table VI. Spatial and energy resolution in the Borexino detector.

| Spatial and Energy Resolution | | |
|---|---|---|
| Energy (MeV) | $\Delta R$ ($\sigma$ (cm)) | $\Delta E$ (FWHM (keV)) |
| 0.05 | 71.6 | 36.9 |
| 0.1 | 52.3 | 54.2 |
| 0.2 | 35.2 | 73.6 |
| 0.5 | 18.3 | 116.3 |
| 1.0 | 12.9 | 176.1 |
| 2.0 | 9.9 | 276.2 |
| 4.0 | 9.7 | 436.1 |
| 5.0 | 10.2 | 524.2 |
| 6.0 | 10.3 | 612.3 |

## 9.2 - SYSTEMATIC ERRORS

Let us suppose that there is not light scattering in the liquid scintillator. The mean value of the $PMT$ time signals has a systematic error due to the spatial distribution of the $PMT$ positions. The $PMT$'s are uniformly distributed on the surface of a sphere. If the scintillation photons of a point source are generated at $t_0$ time then the mean value of the $PMT$ time signals is given by

$$\bar{t} = t_0 + \Delta\bar{t} \,,$$

where $\Delta\bar{t}$ is given by the formula:

$$\Delta\bar{t} = R\left(1 + \frac{d^2}{3R^2}\right)\frac{n}{c}$$

formula, where $R$ is the detector radius, $d$ is the distance between the point source and the center of the detector, $n$ is the refractive index of the material and $c$ is the speed of light.

## 9.3 - MULTIPLE HITS

A high energy particles produce a lot of photons ($\sim$ 5000 photons/MeV). If the number of produced photons is big, then there are $PMT$'s which detect more than one photons from the event (multiople hit). The multiple hits have a significant influence on the accuracy of the event reconstruction. The number of detected scintillation photons and the number of the hit photomultiplier tubes depends on the deposited energy and on the distance between the energy deposit and the detector centre. The distribution of single, double etc. hits are given in Table VII in the case of the Borexino detector. At small energies the number of multiple hits is negligible and the vertex error decreases with the energy except that at high energies where the error is constant (Table VI).

Table VII. Distribution of multiple hits in Borexino

| Distribution of Multiple Hits in Borexino | | | | | | |
|---|---|---|---|---|---|---|
| Energy deposit (MeV) | single (%) | double (%) | triple (%) | fourfold (%) | fivefold (%) | >fivefold (%) |
| 0.05 | 99.14 | 0.86 | | | | |
| 0.1 | 98.43 | 1.57 | | | | |
| 0.2 | 97.17 | 2.68 | 0.12 | 0.03 | | |
| 0.8 | 88.95 | 9.69 | 1.21 | 0.14 | 0.01 | |
| 5.0 | 57.45 | 24.64 | 9.73 | 4.18 | 2.01 | 1.99 |
| 10.0 | 37.55 | 26.76 | 15.14 | 8.41 | 4.62 | 7.52 |

## 10 - REFERENCES

[1] Borexino at Gran Sasso, Proposal for a Real Time Detector for Low Energy Solar Neutrinos (August 1991), Edited by G.Bellini, M.Campanella, D.Giugni, Dept. of Physics of University of Milano and I.N.F.N. - Milano and R.S.Raghavan, AT&T Bell Laboratories (August 1991)

[2] W.R.Nelson et al., The *EGS* Code System, SLAC Report 265, December, 1985.

[3] M.Born and E.Wolf. Principles of Optics. Pergamon, 1964

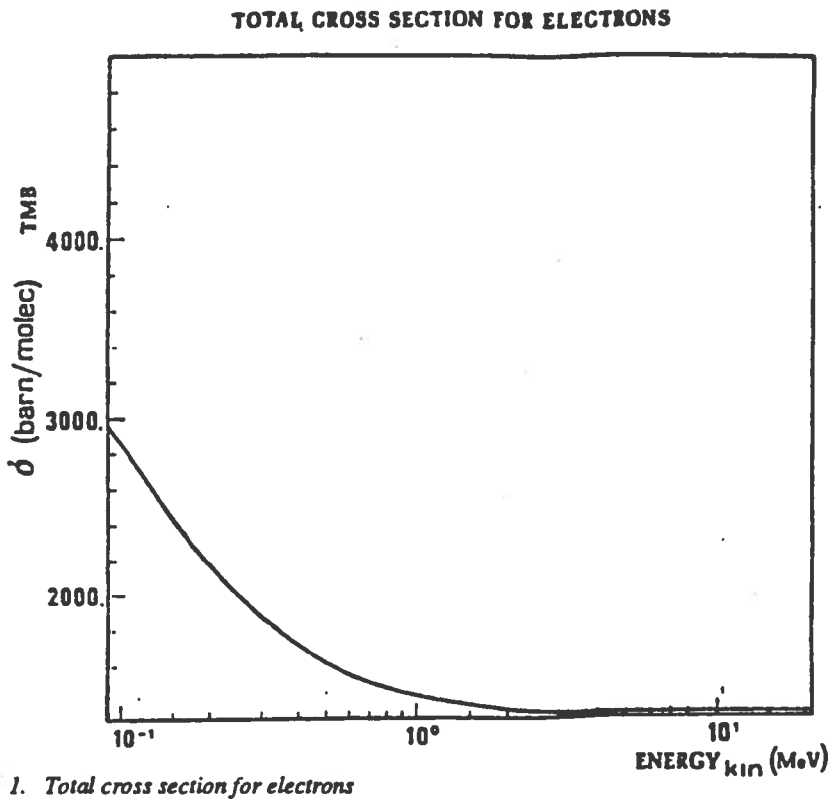


*Figure 1. Total cross section for electrons*

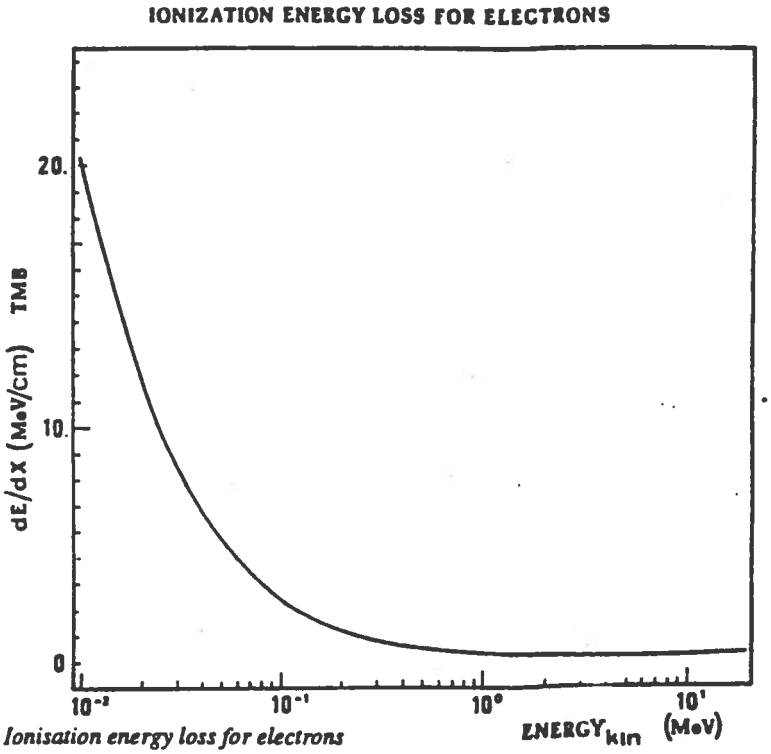


*Figure 2 Ionisation energy loss for electrons*

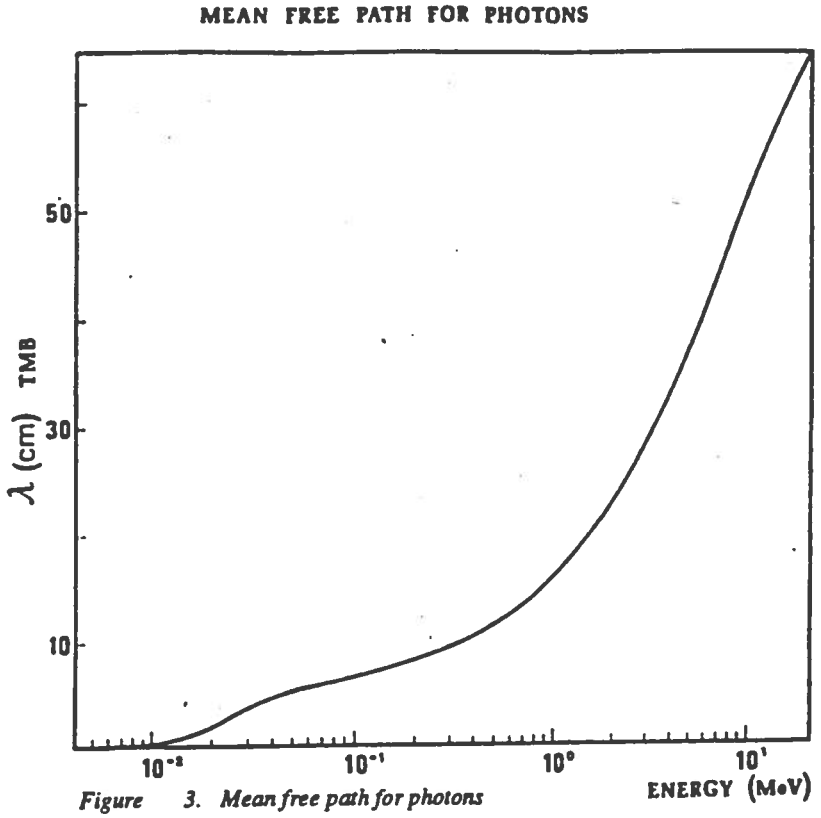


*Figure 3. Mean free path for photons*

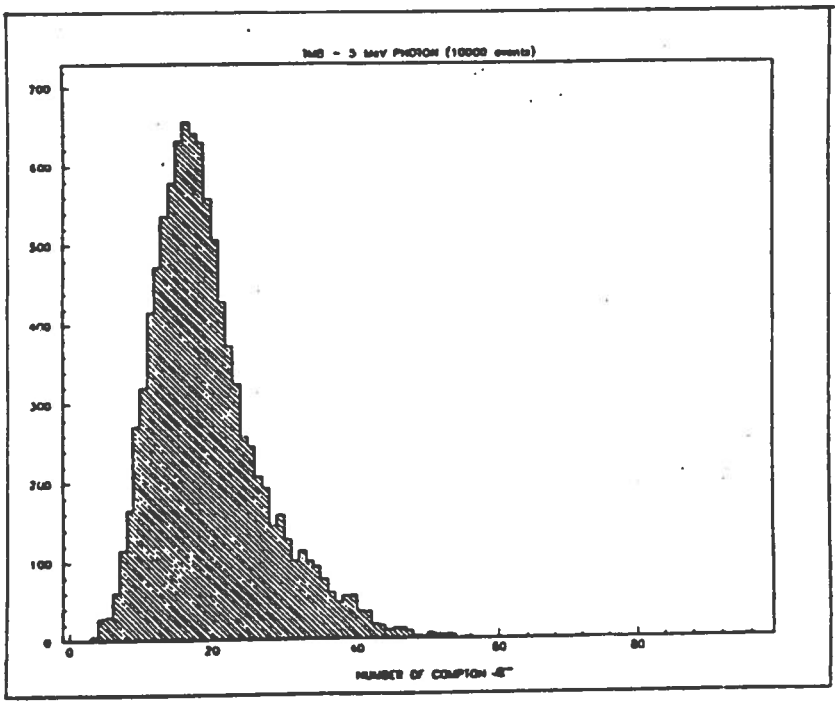


*Figure 4. Distribution of Compton electrons per event originated by a 5 MeV photon*

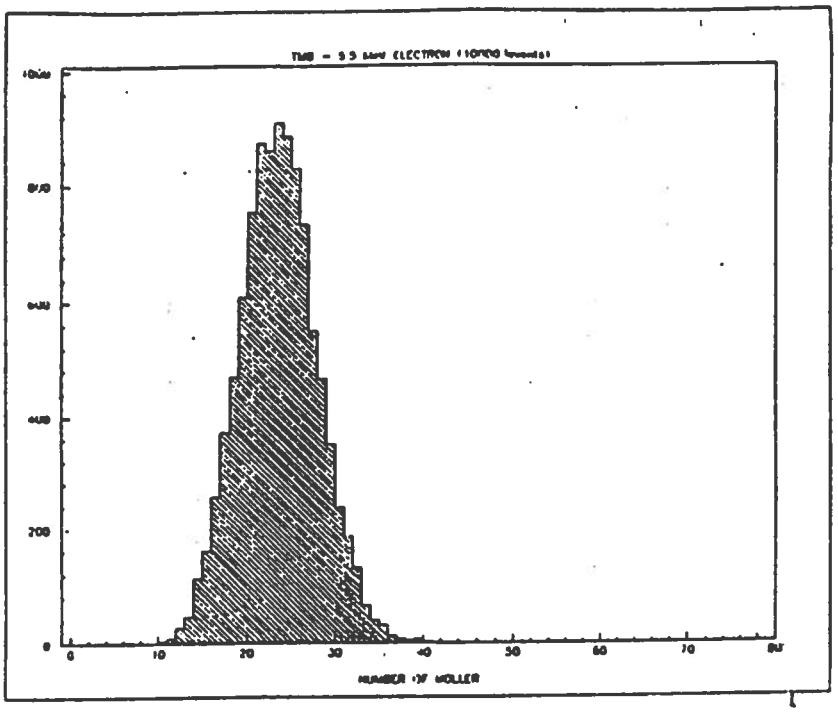

*Figure 5a. Distribution of Möller electrons per event originated by a 5.5 MeV electron*

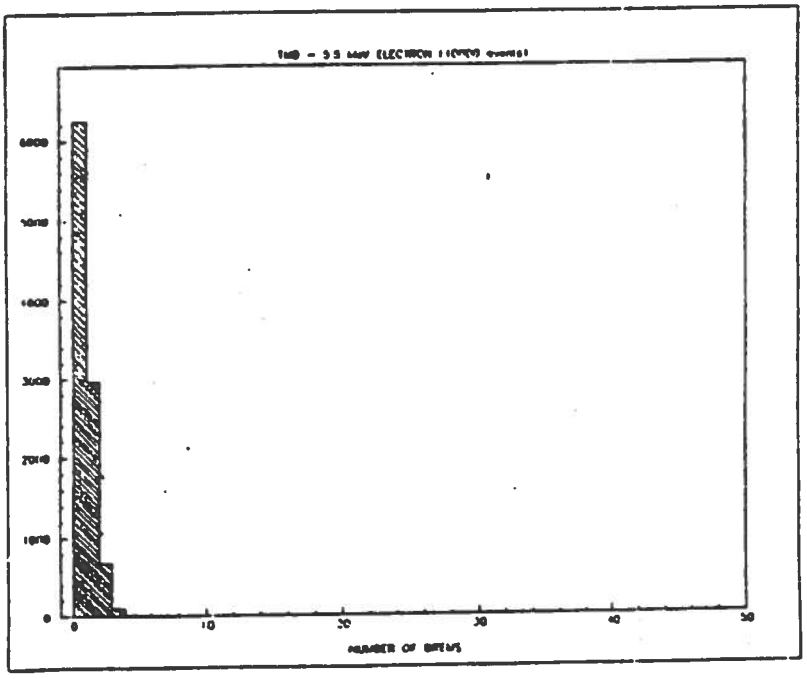

*Figure 5b. Distribution of Bremsstrahlung photons per incident electron of 5.5 MeV*

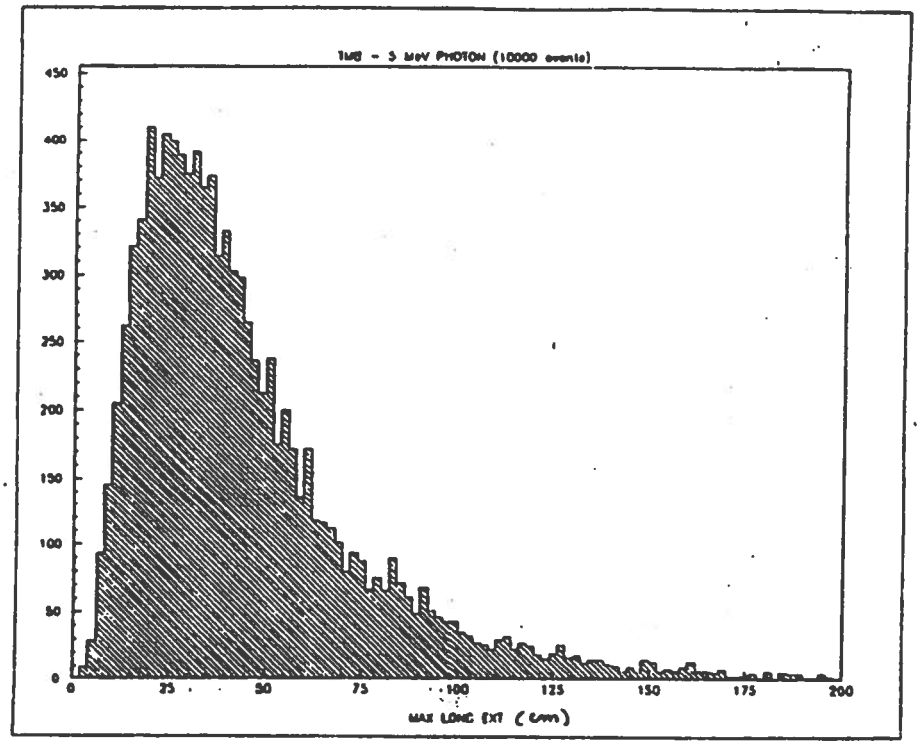


*Figure 6a. Distribution of the maximum longitudinal extension of showers originated by 5 MeV photons*

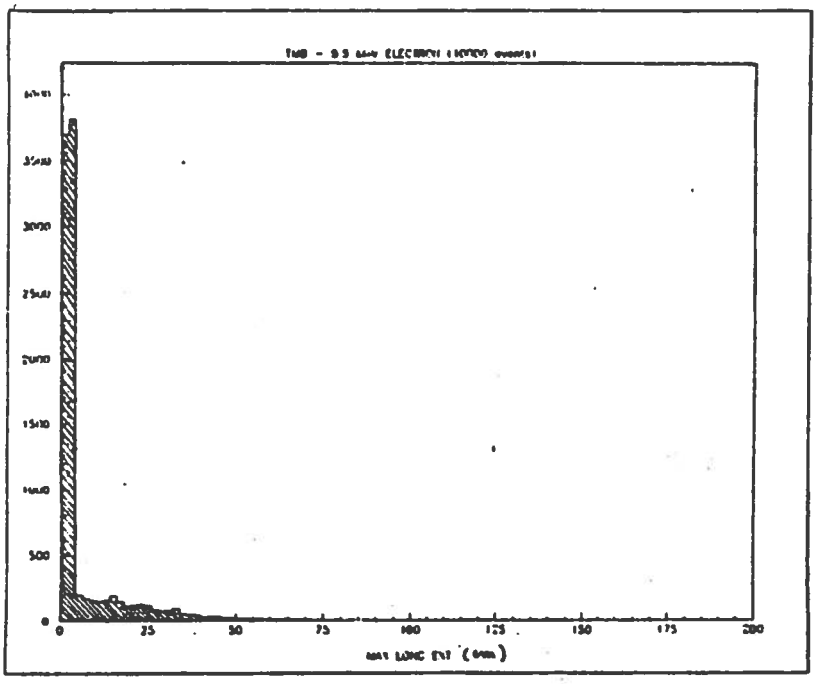


*Figure 6b. Distribution of the maximum longitudinal extension of showers originated by 5.5 MeV electrons*

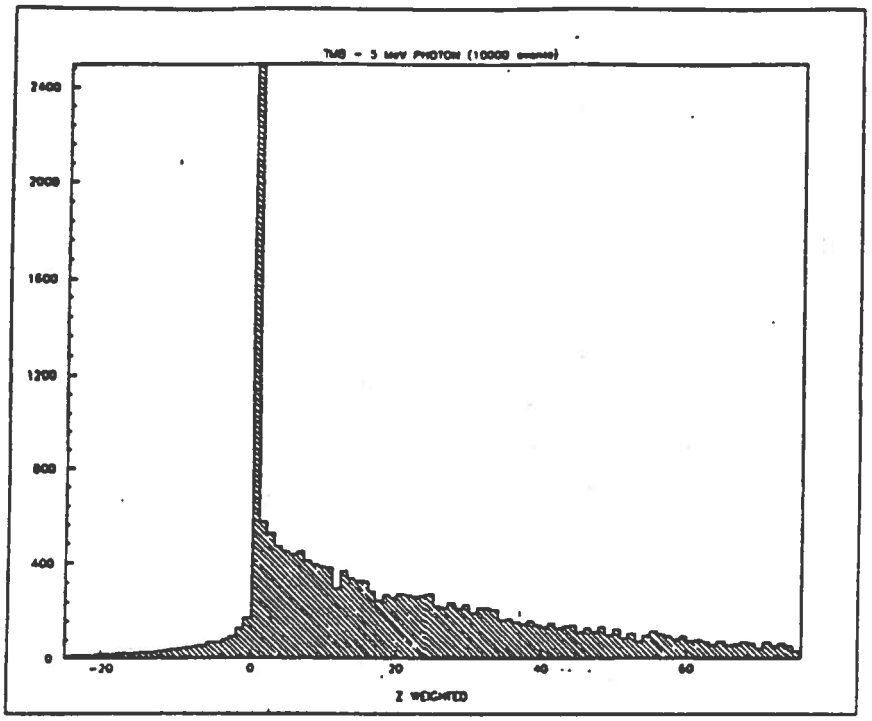


*Figure 7a. Spatial distribution of the deposited energy for 5 MeV photons*

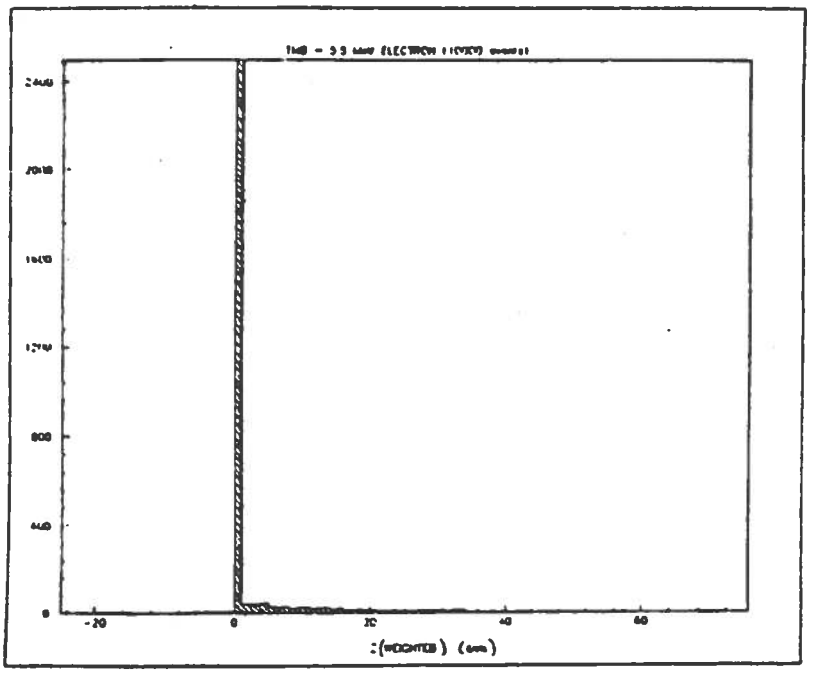

*Figure 7b. Spatial distribution of the deposited energy for 5.5 MeV electrons*

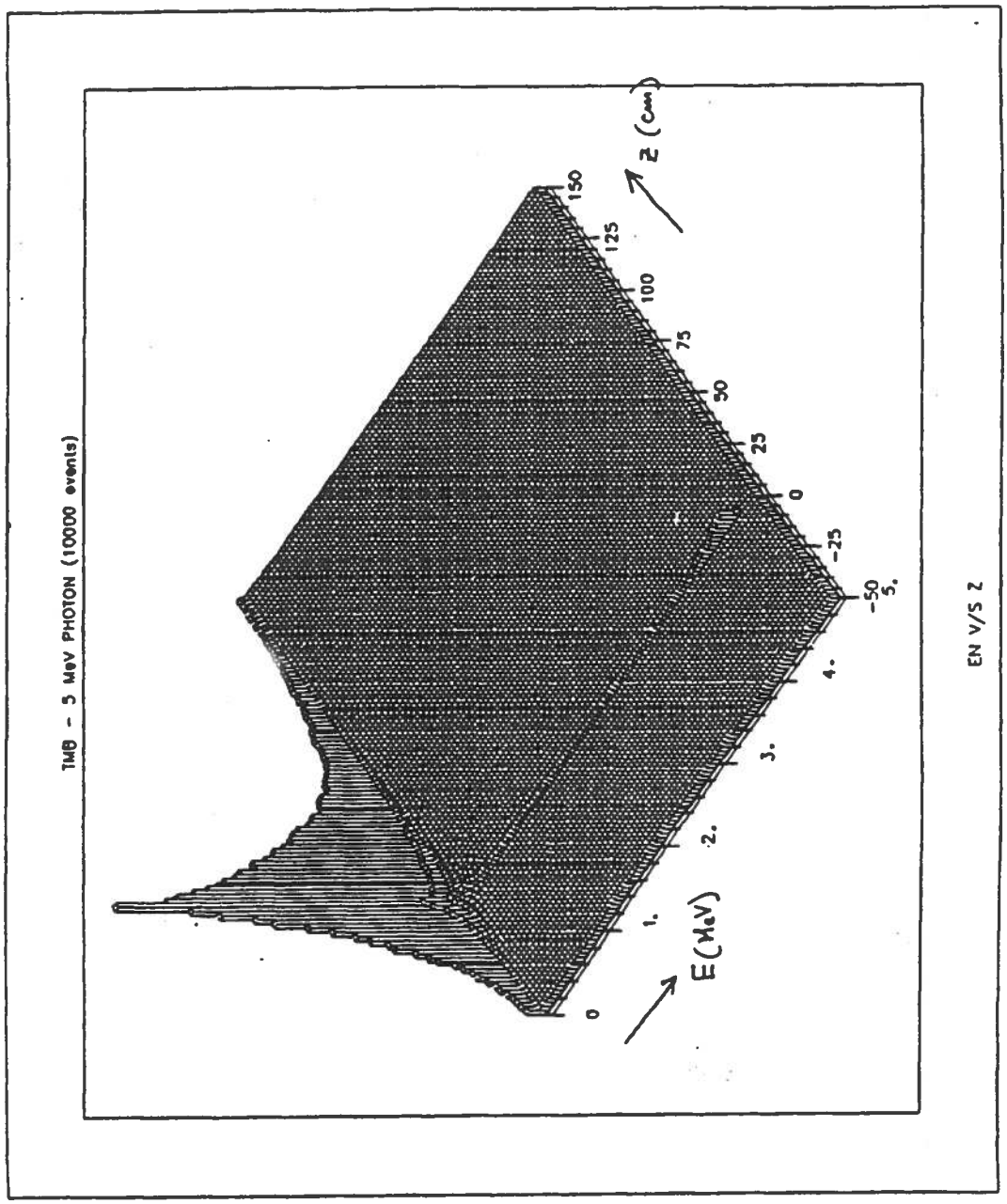


*Figure 8a. Spatial distribution of the deposited energy in a (z,E) plane for 5 MeV photons [z is the coordinate along the longitudinal extension of the shower]*

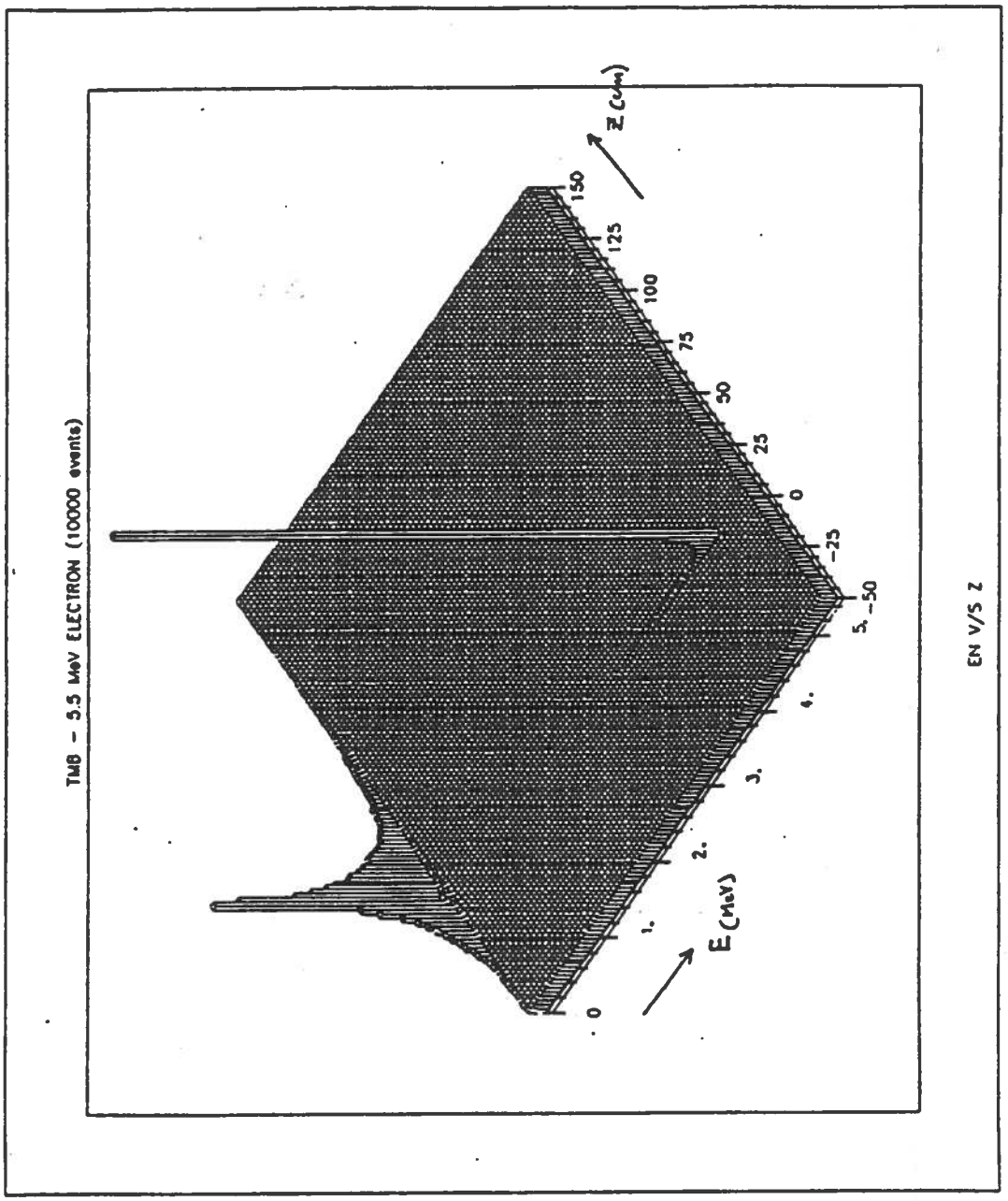


*Figure 8b. Spatial distribution of the deposited energy for 5.5 MeV electrons in a (z, E) plane*

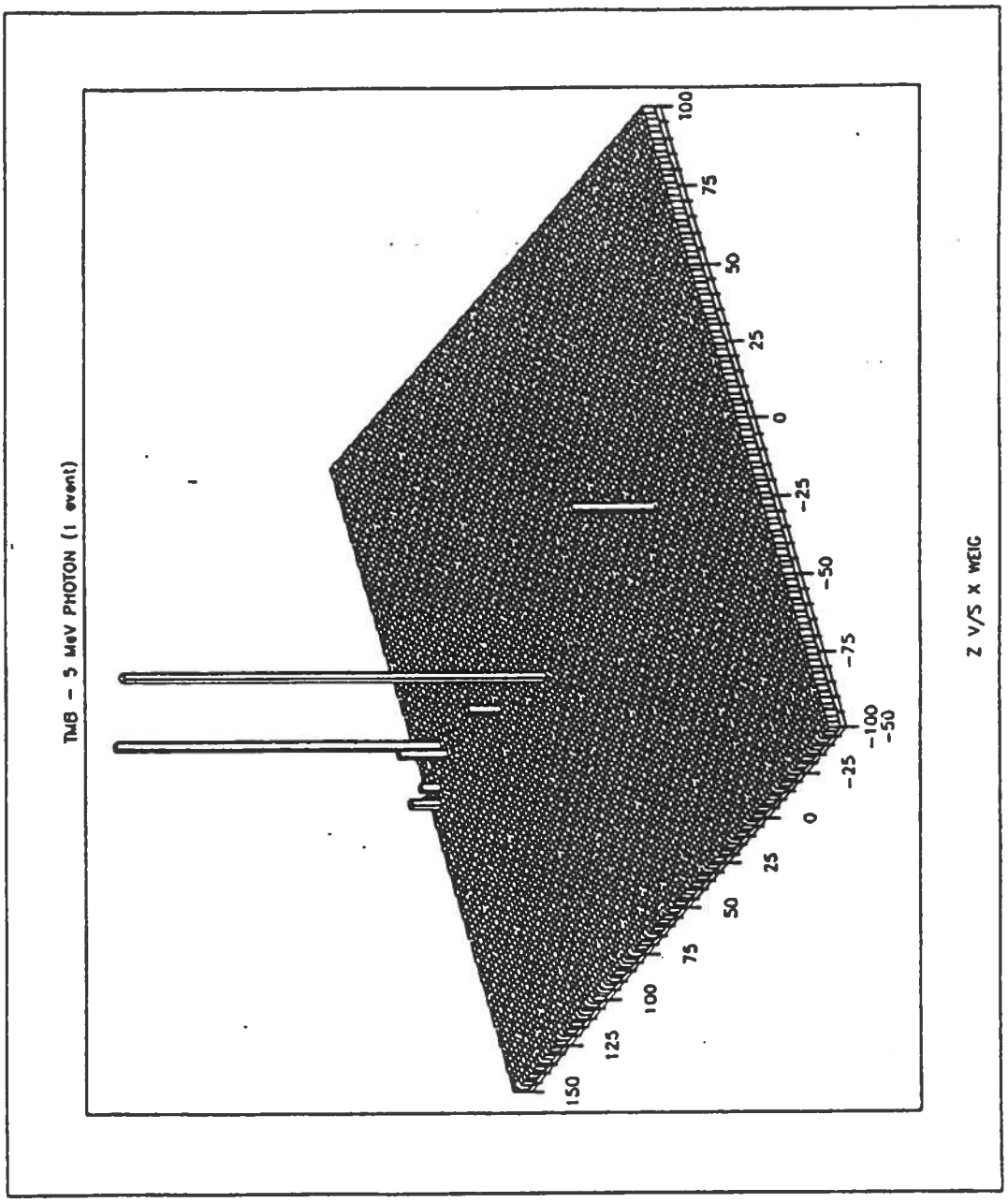


*Figure 9. The energy deposited by a single 5 MeV photon in a plane parallel to the incident direction*

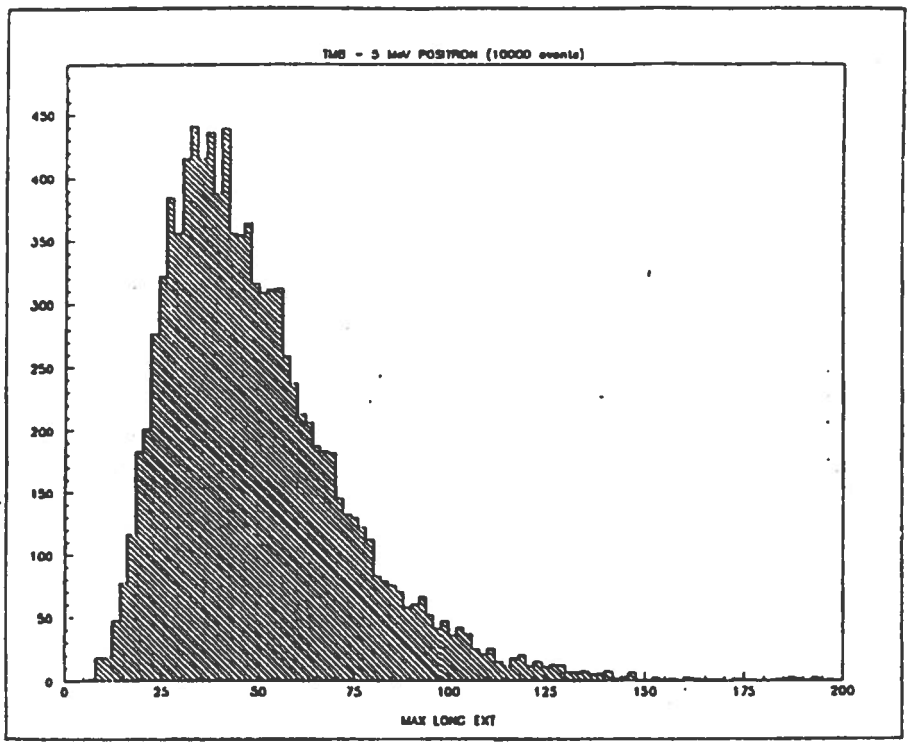


*Figure 10a. Distribution of the maximum longitudinal extension of showers originated by 5 MeV positrons*

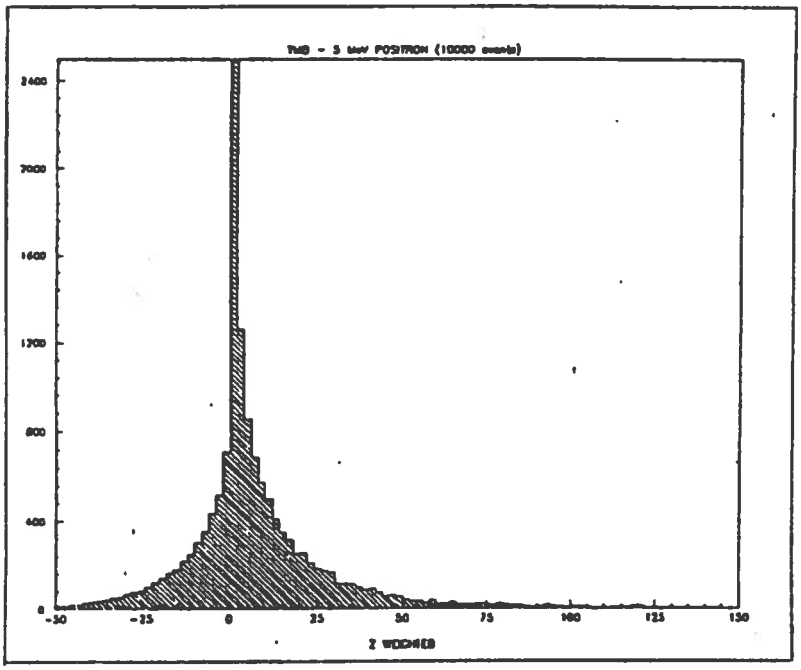


*Figure 10b. Spatial distribution of the deposited energy for 5 MeV positrons*

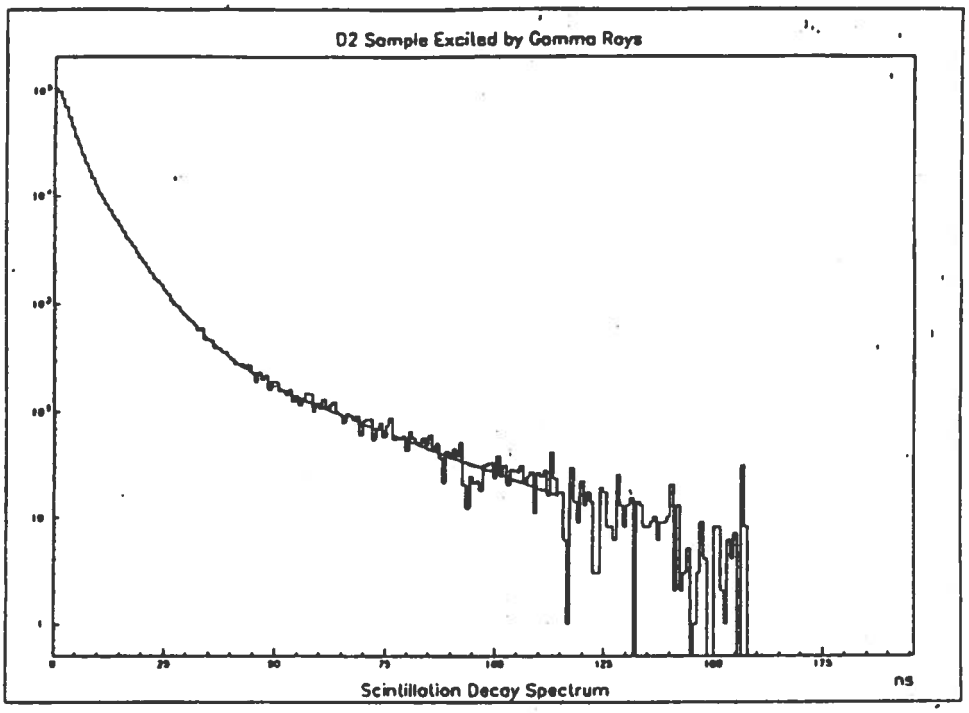


*Figure 11 Decay spectrum of the scintillator D2. The scintillator was excited by gamma rays*

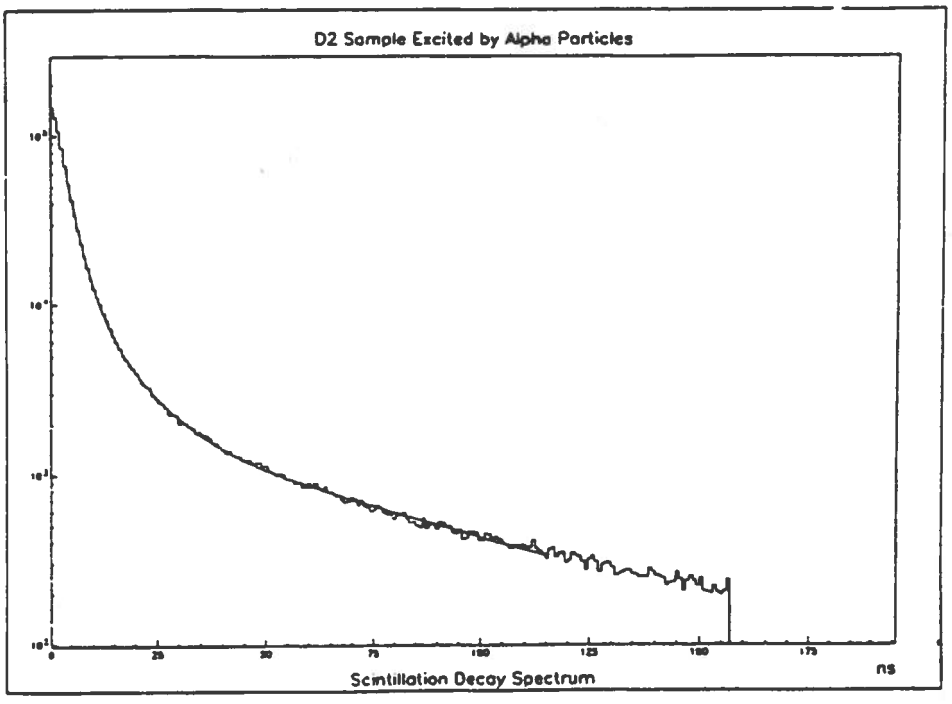


*Figure 12. Decay spectrum of the scintillator D2. The scintillator was excited by α particles*

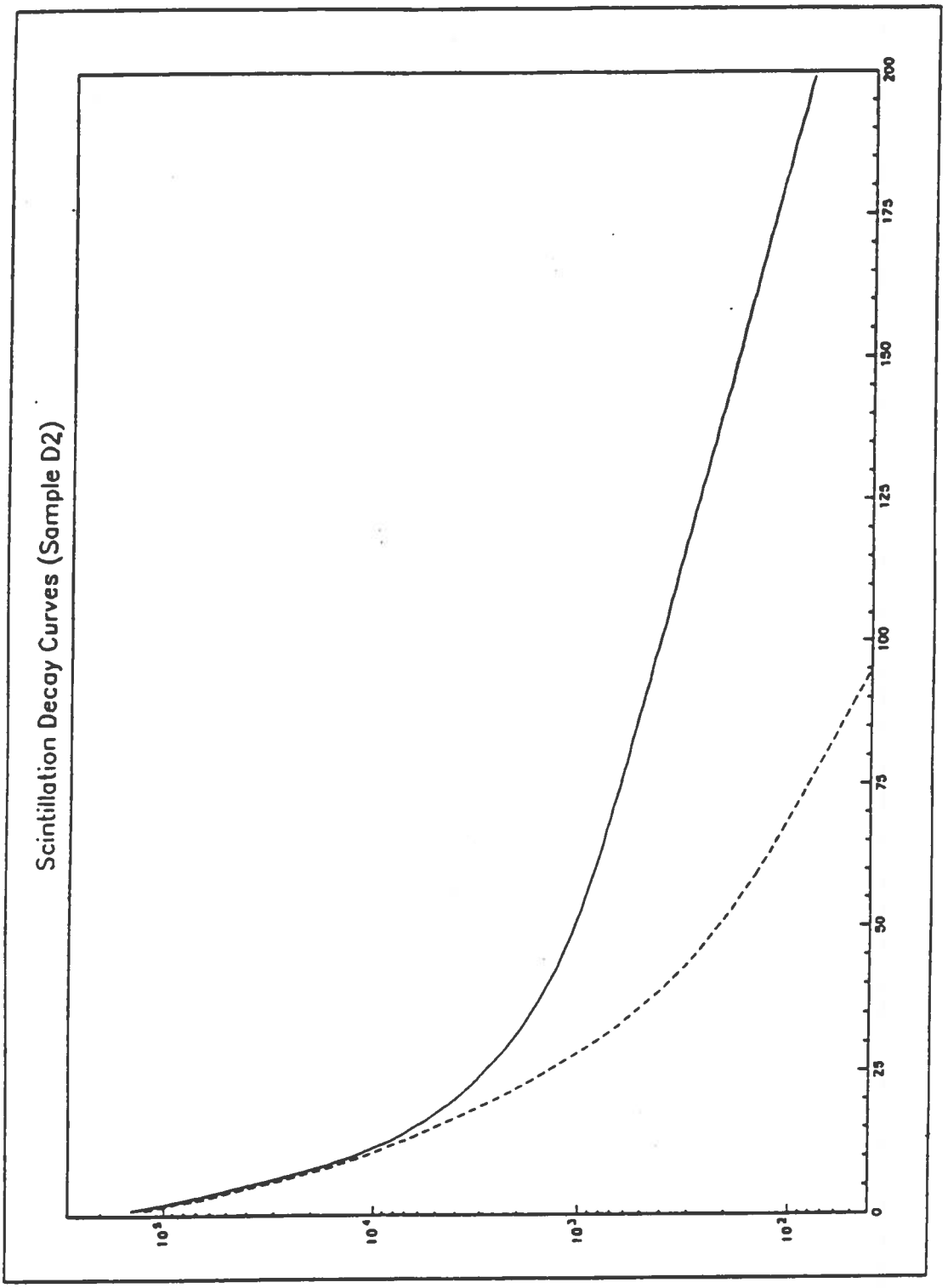


*Figure 13. Scintillator decay curves. The sum of three exponentials were fitted to the decay spectrums of the scintillator D2.*

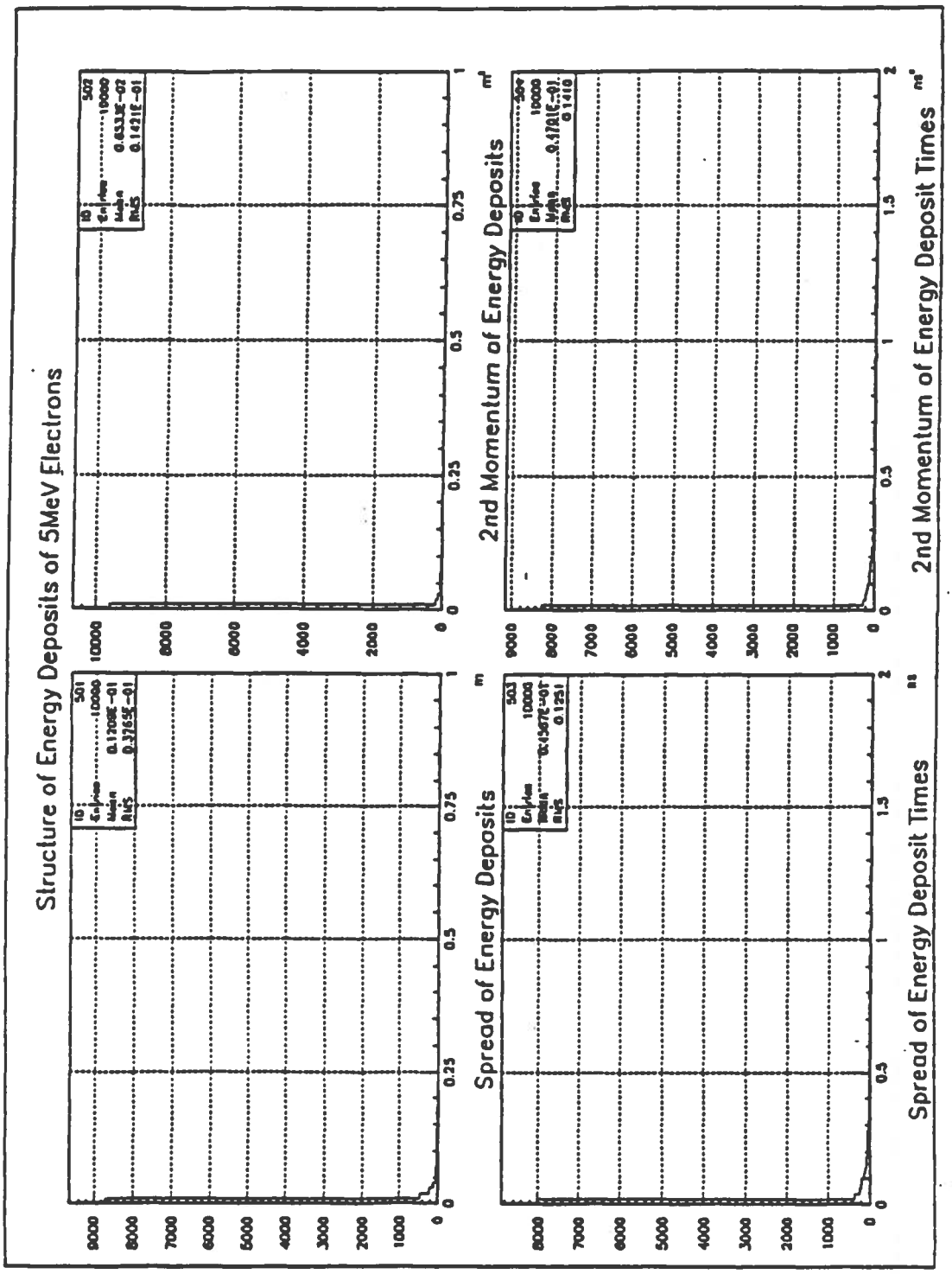


*Figure 14. Distributions of the energy deposits produced by 5 MeV electrons*

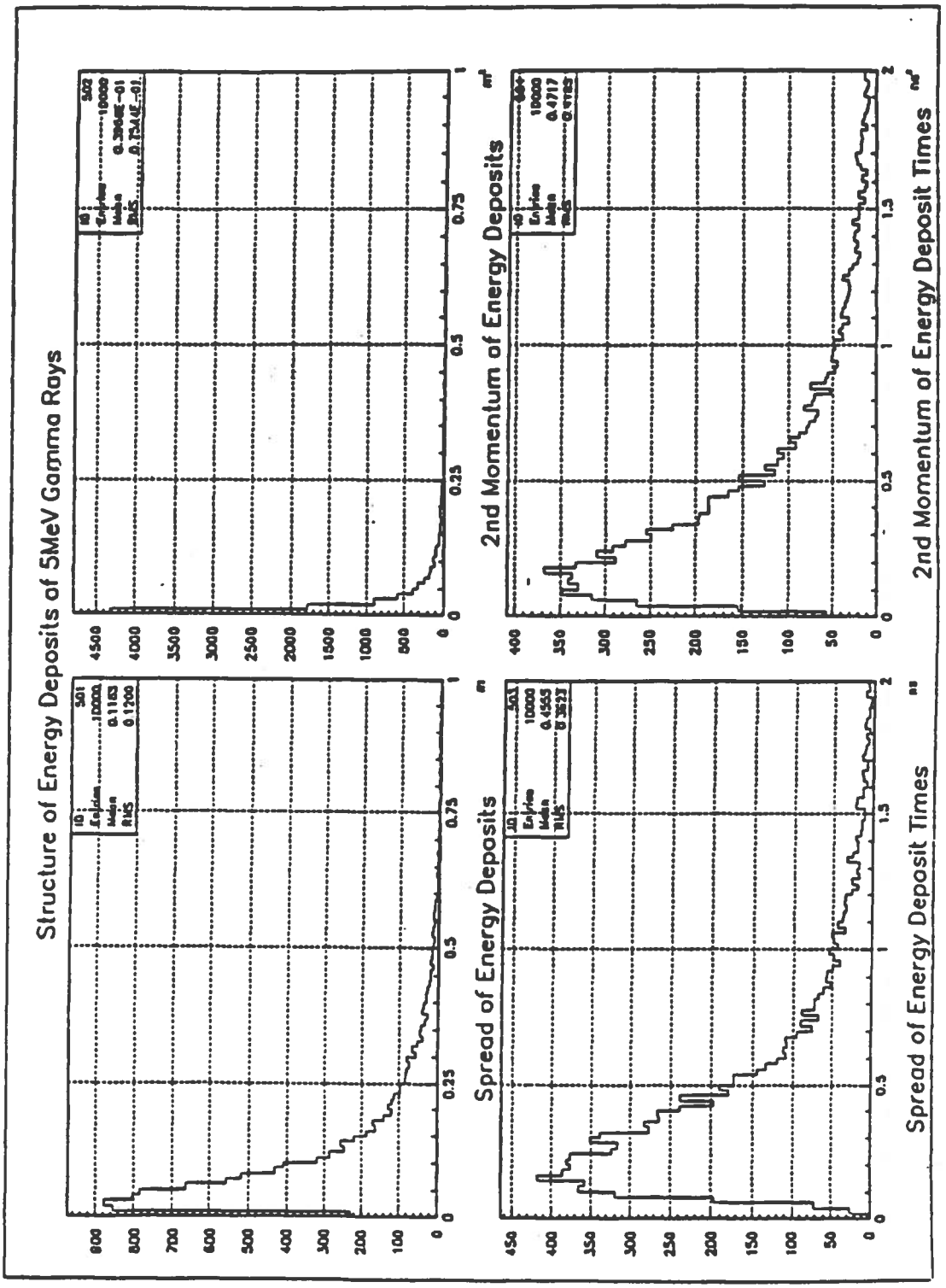


*Figure 15. Distributions of the energy deposits produced by 5 MeV gamma rays*

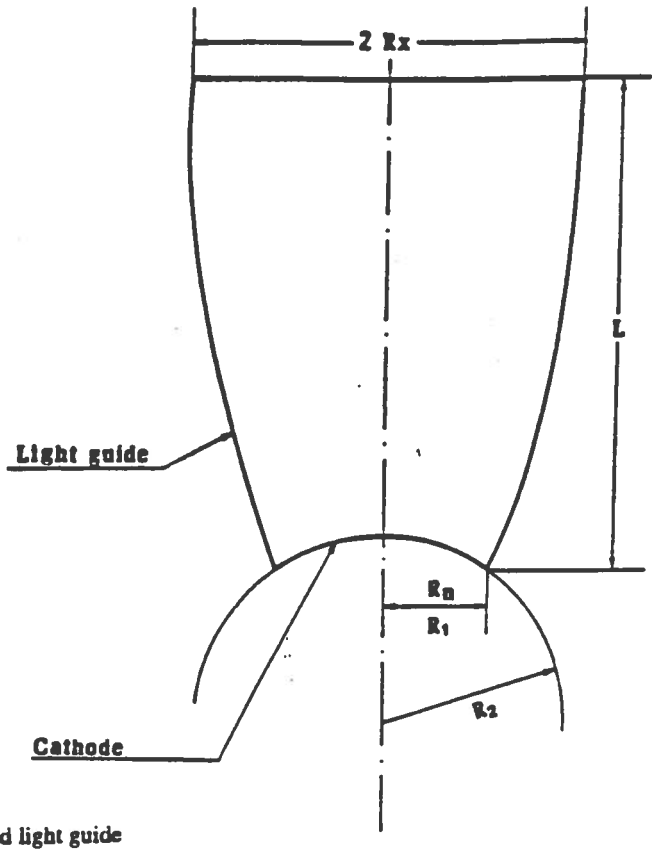


*Figure 16.*
**Parabola-shaped light guide**

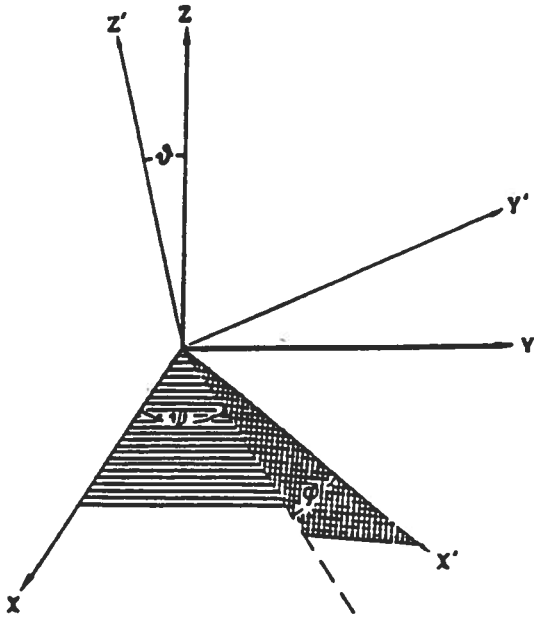


*Figure 17.* **Orthogonal coordinate systems and Euler angles**

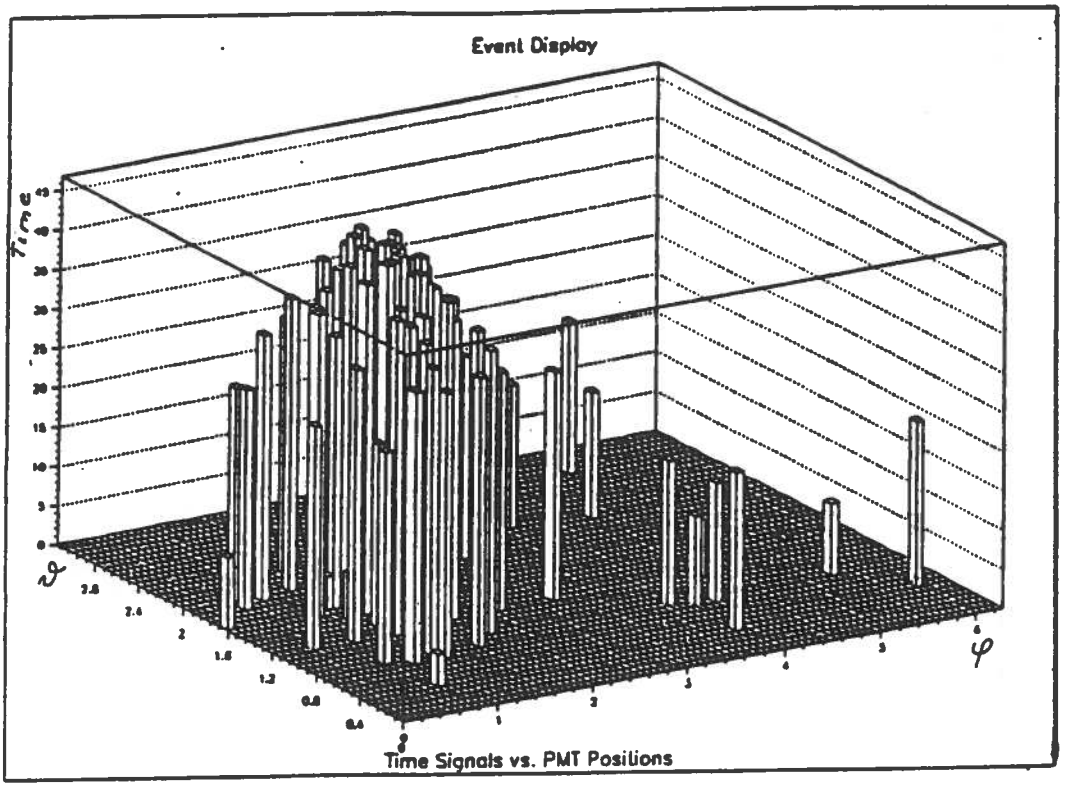


*Figure 18. Event display. The time signals of point-sized energy deposit are displayed as a function of the PMT* positions

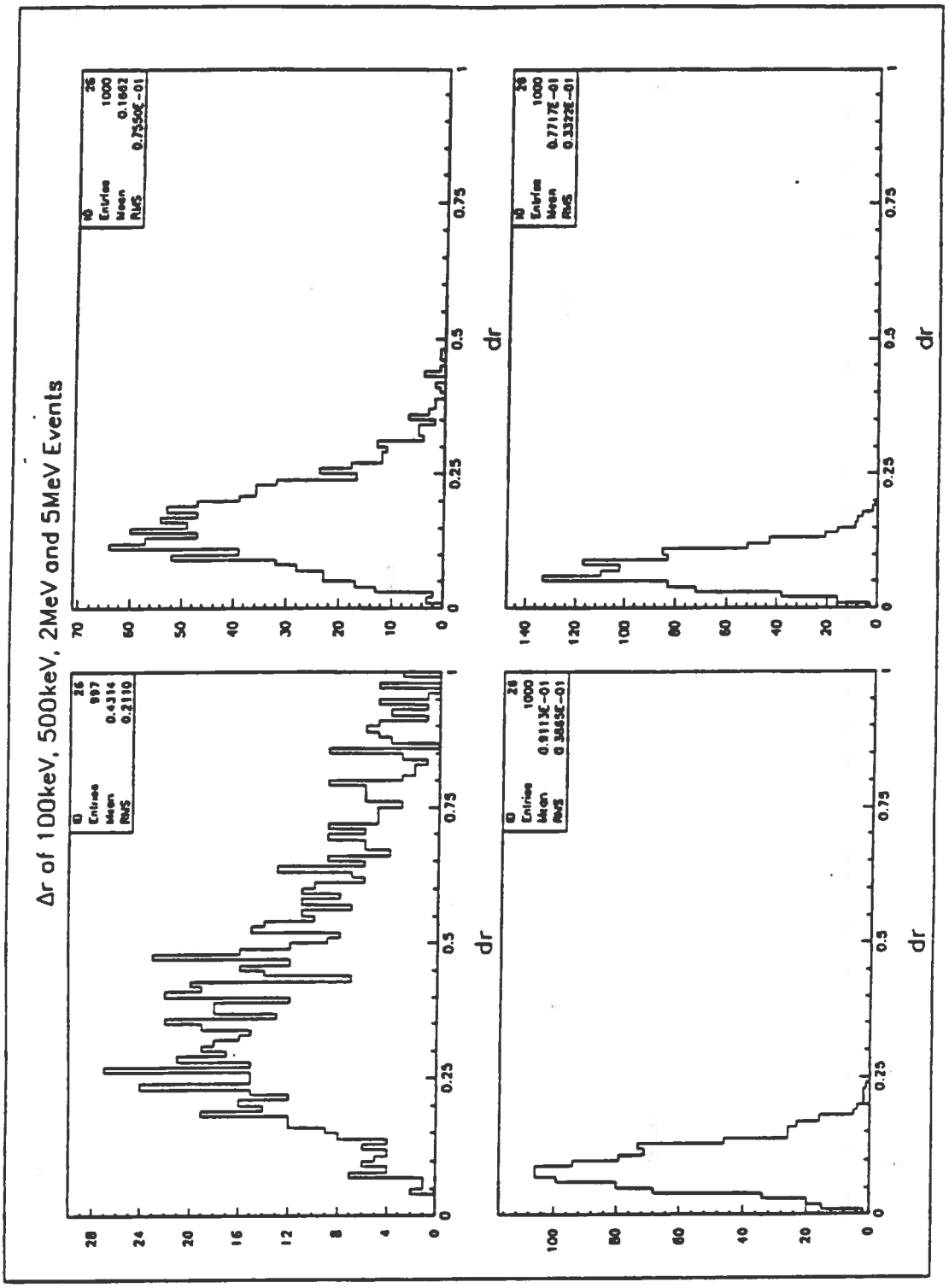


*Figure 19. Errors of the vertex reconstruction. The 100keV, 500keV, 1MeV and 5MeV point-sized energy deposits were distributed uniformly in the fiducial volume*

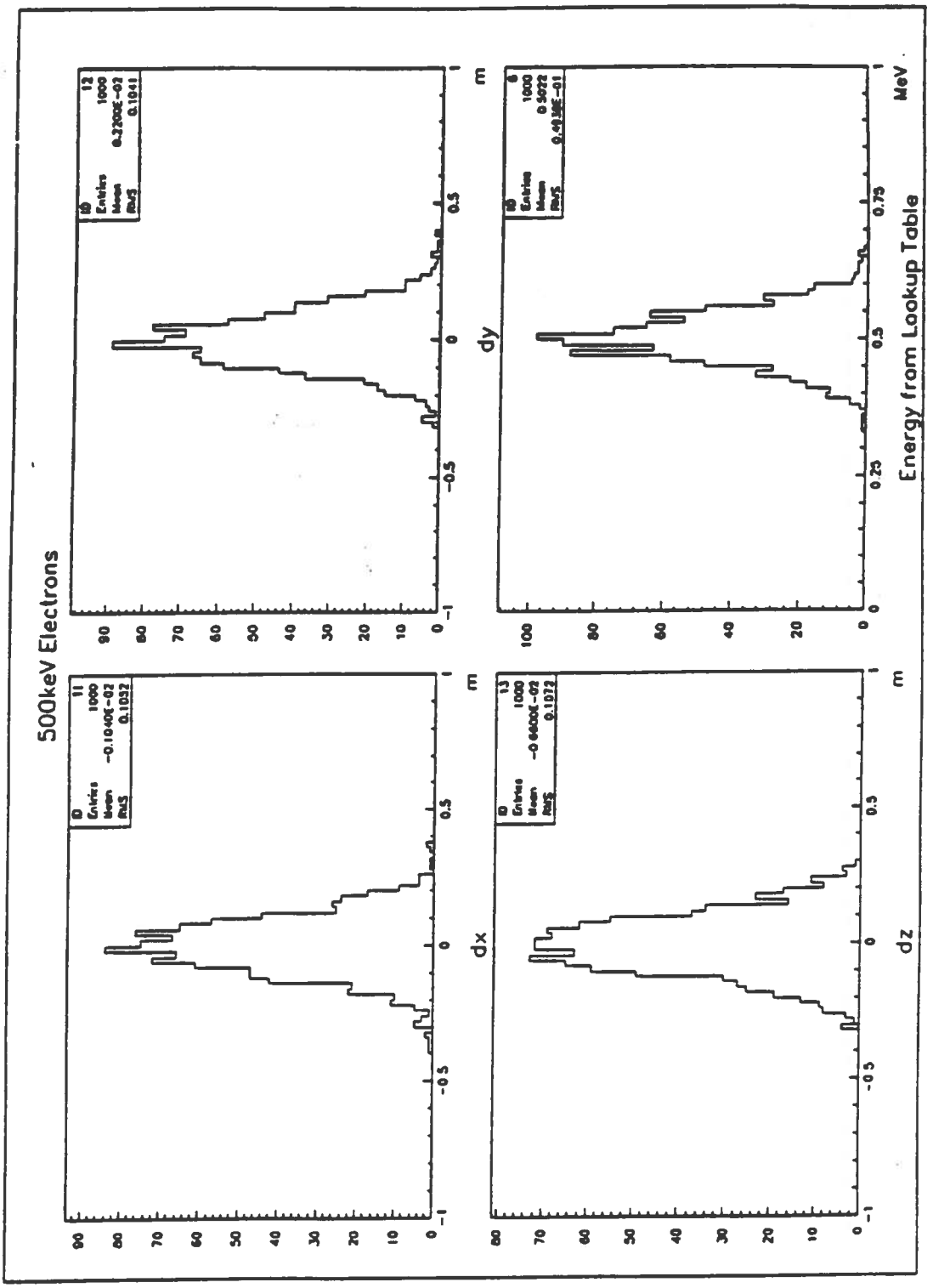


*Figure 20. Spatial and energy resolution. The 500 keV point-sized energy deposits were distributed uniformly in the fiducial volume.*

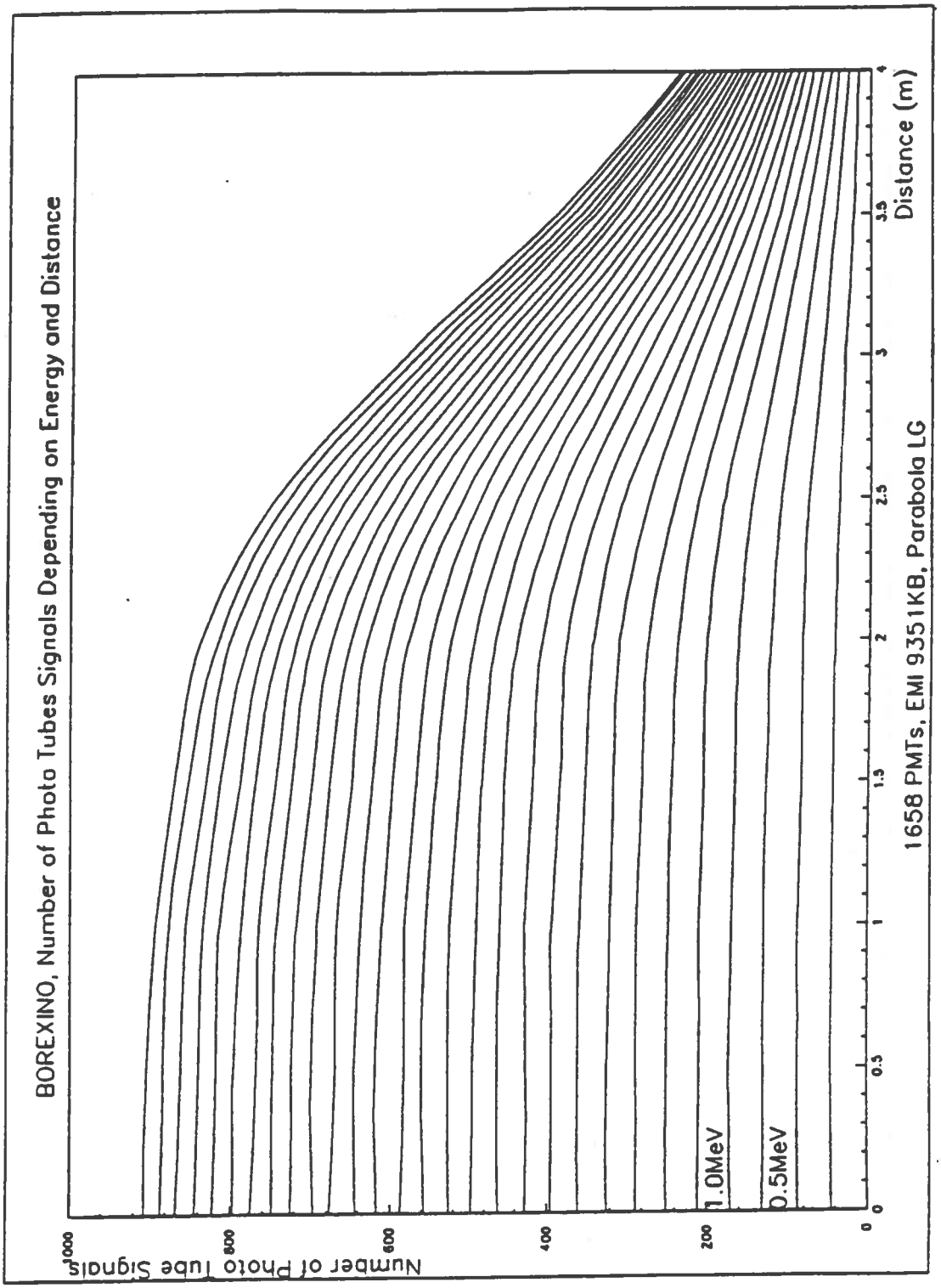


*Figure 21. The number of the photomultiplier tube signals vs. the deposited energy and the distance between the energy deposit and the detector centre*

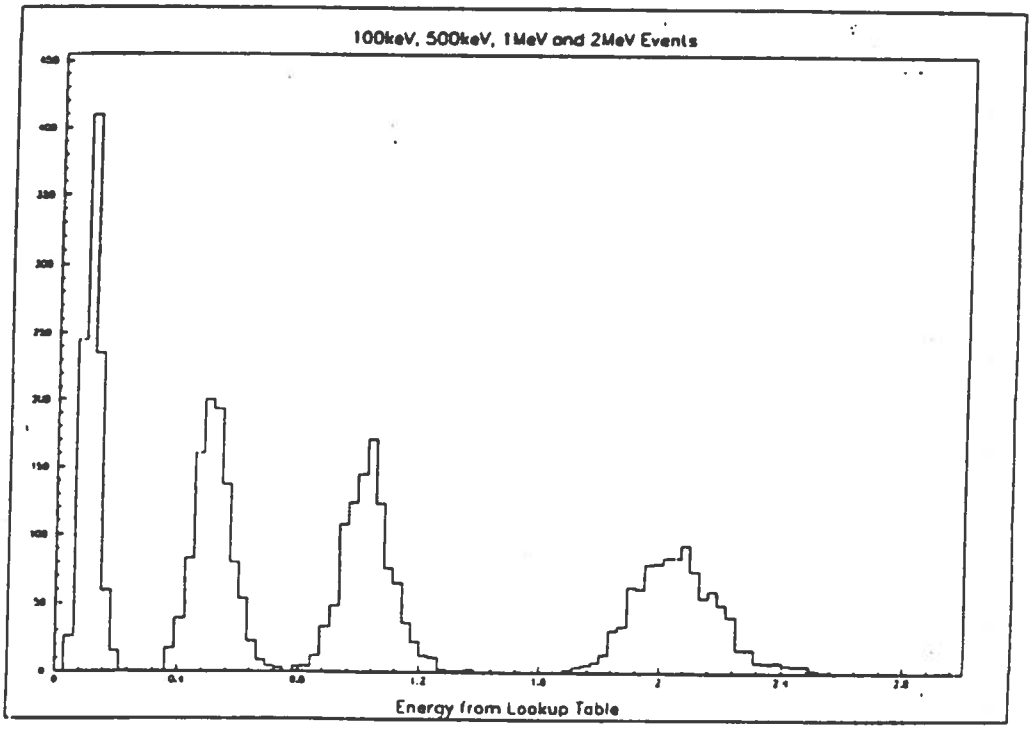


*Figure 22. Energy resolution. The 100 keV, 500 keV, 1 MeV and 2 MeV point-sized energy deposits*